Raman spectrum of superconducting oxides

A. Virosztek
Central Research Institute for Physics, H-1525 Budapest 114, P.O. Box 49, Hungary

J. Ruvalds
Physics Department, University of Virginia, Charlottesville, Virginia 22901
(Received 28 May 1991; revised manuscript received 12 August 1991)

The anomalous electronic Raman scattering in the normal state of various cuprates extends smoothly to an energy of 1 eV. This behavior is shown to be in accord with the frequency-dependent damping caused by electron-electron scattering between nearly parallel (i.e., "nested") sections of the Fermi surface. Intermediate on-site Coulomb repulsion is found to be compatible with the data, whereas the long-range Coulomb coupling is ineffective in the small-momentum-transfer limit. The matrix element for the scattering process is attributed to energy-density fluctuations for anisotropic Fermi surfaces. By contrast, conventional density-fluctuation processes for parabolic energy bands are several orders of magnitude smaller and restricted to a narrow frequency range because of charge conservation and the Pauli exclusion principle. A surprising proportionality between the Raman line shape and the optical conductivity is derived in the nesting approximation. Evidence for such behavior is established by fits to the Raman spectra of $YBa_2Cu_3O_7$ and $Bi_2Sr_2CaCu_2O_8$ using electron-electron coupling and energy-cutoff values previously obtained from our analysis of the optical conductivity and reflectance data. Similar electronic spectra should appear in other metals with nested Fermi surfaces, such as chromium and various rare-earth metals.

I. INTRODUCTION

Raman scattering by single-particle excitations in a simple metal is expected to be very weak and restricted to frequencies below 30 cm^{-1} for ordinary laser probes and Fermi velocities. The cross section is proportional to the Fermion gas structure factor[1] $S(\mathbf{q},\omega)$ which tends to vanish as $\mathbf{q}\rightarrow\mathbf{0}$, and is surely very small at the momentum transfer $\mathbf{q}$ of the light.

Thus the discovery[2,3] of strong electronic Raman scattering over a wide frequency range in $YBa_2Cu_3O_7$ generated a fundamental theoretical challenge which may have relevance to the high superconducting transition temperatures of the cuprates. The insulating counterpart $YBa_2Cu_3O_6$ exhibits a Raman spectrum of similar intensity and range, but the antiferromagnetism in this case produces a much different line shape with a broad peak which has been established as two-magnon scattering.[4]

Similar flat Raman spectra have been observed for other cuprates and in the unusual superconductor[5] $Ba_xK_{1-x}BiO_3$ which does not have spin fluctuations of the form usually associated with the copper oxides. The slight frequency variation of the electronic spectrum of the superconductors is sensitive to the light polarization.[6]

Metals with anisotropic Fermi surfaces allow light to couple to fluctuations in the energy density[7] and thereby yield a quasielastic continuum that is much different than the weaker charge density scattering. The nonparabolic band scattering originally derived for doped semiconductors may be applicable to superconductors[8] with particular relevance to the layered copper oxide superconductors.[9] The acceleration of an electron by an optical field creates a change in the effective mass which introduces a nonlinear term in the equation of motion.

The anomalous Raman scattering data in the cuprates provided the inspiration for the "marginal Fermi liquid" hypothesis[10] which presumed that the susceptibility at long wavelengths has the form $\chi''_M \propto \omega/T$ for $|\omega| < T$ and $\chi''_M \propto \mathrm{sgn}(\omega)$ for $|\omega| > T$. Considering the standard Bose factor in the cross section, this phenomological form of χ''_M was inferred from a flat Raman spectrum. Assuming further that this χ''_M structure is independent of momentum $\mathbf{q}$, it generates a quasiparticle self-energy $\Sigma''_M \propto \max(T,|\omega|)$ that is claimed to be compatible with conductivity and other measurements on the cuprates. However, if the linear frequency variation continues to zero frequency and temperature, the corresponding singularity in the effective mass leads to a breakdown of conventional Fermi-liquid (FL) behavior, and this situation has been named "marginal."

The purpose of the present work is to calculate the electronic Raman response of a nested Fermi liquid (NFL) which is characterized by nearly parallel sections of electron (or hole) orbits.[11] The optical response of the NFL model is much different from conventional Drude behavior, and yields a remarkably good description of conductivity and reflectivity data on high-temperature superconductors with an on-site Coulomb coupling comparable to the bandwidth.[12] Our Raman calculation of the energy density response includes self-energy and vertex corrections from electron-electron scattering. The magnitude and unusual linear frequency variation of the NFL damping provides the mechanism for light scattering out to large frequencies (~ 1 eV).

In relation to Raman scattering it is instructive to first present the structure factor in the NFL theory using the standard relation[1]

$$S(\mathbf{q},\omega)=\frac{-q^2}{4\pi e^2}\,\mathrm{Im}\frac{1}{\epsilon(\mathbf{q},\omega)}\ , \tag{1}$$

where the dielectric function in the long-wavelength limit $\mathbf{q}\to\mathbf{0}$ is given by[12]

$$\epsilon_{\mathrm{NFL}}(\omega)=\epsilon_\infty-\frac{\omega_{\mathrm{pl}}^2}{\omega[\omega m^*/m_0+i/\tau_{\mathrm{NFL}}(\omega)]}\ . \tag{2}$$

The plasma frequency ω_{pl} is found to be near 3 eV for superconducting $Bi_2Sr_2CaCu_2O_8$ using the above form to fit data[13] on infrared conductivity, reflectivity, and the f-sum rules for the conductivity as well as the structure factor.[14] The key ingredient in the NFL analysis is electron-electron scattering across regions of the Fermi surface that satisfy the nesting condition

$$E(\mathbf{k}+\mathbf{Q})\cong -E(\mathbf{k}) \tag{3}$$

for a nesting wave vector $\mathbf{Q}$. This approximation yields a quasiparticle transport damping rate that is linear in frequency

$$\frac{1}{\tau_{\mathrm{NFL}}}=\alpha|\omega| \tag{4a}$$

for $\omega>\beta' T$ and also

$$\frac{1}{\tau_{\mathrm{NFL}}}\cong\beta'\alpha T \tag{4b}$$

in the static limit $\omega\ll\beta' T$. The coefficient β' varies from 3.3 in the weak-coupling limit to 4.2 in the strong-coupling limit[12] where α is proportional to the Coulomb coupling U divided by the bandwidth W. Specific analysis of the $Bi_2Sr_2CaCu_2O_8$ data reveals $\alpha\simeq 0.4$, which is compatible with a Boltzmann equation solution if $U/W=1.0$ and 90% of the Fermi surface satisfies the nesting condition.[14] Physically, the finite transport damping for electron-electron collisions on a nested surface originates form an anisotropic velocity distribution along the orbit that permits a current change despite momentum conservation.

The structure factor $S_{\mathrm{NFL}}(\mathbf{q},\omega)$ corresponding to the above NFL analysis exhibits a broad plasmon peak as shown in Fig. 1: The line shape at low and intermediate ($\omega\sim 1$ eV) frequencies is quite close to the spectrum derived from optical reflectivity data[13] and is generally compatible with independent electron loss measurements[15] performed at a momentum transfer $|\mathbf{q}|\cong 0.05$ Å^{-1}. The $S_{\mathrm{NFL}}(\mathbf{q},\omega)$ function satisfies the f-sum rules required by charge conservation, although there is some uncertainty near the cutoff in the 2-eV range.

Clearly the structure factor deduced in Fig. 1 is *not* seen in the Raman spectra of the cuprates.[2–6] This is not surprising in view of the small cross section for the isotropic scattering mechanism[1] and the minor influence of the energy fluctuations on the plasmon scattering.[7] Furthermore, the NFL structure factor is much different from the corresponding marginal FL phenomenological

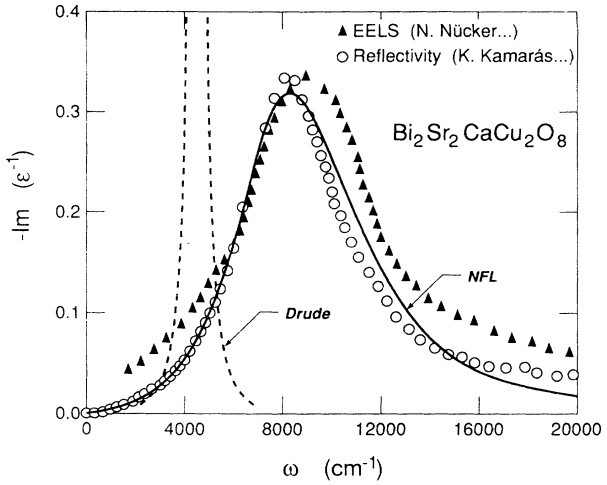

FIG. 1. Structure factor for $Bi_2Sr_2CaCu_2O_8$ derived from optical reflectivity data of Ref. 13 is shown by circles. The calculated NFL loss function is the solid curve obtained with $\epsilon_\infty=5$, $\omega_{\mathrm{pl}}=3.1$ eV, $\alpha=0.4$, and a cutoff $\omega_c\cong 1.2$ eV: This function satisfies the f-sum rules and the evident large plasmon width is caused by the frequency variation of the damp $1/\tau_{\mathrm{NFL}}(\omega)$. Electron loss data from Ref. 15 at $q=0.05$ Å^{-1} is shown by triangles. A conventional Drude fit to the low-frequency conductivity predicts the narrower dashed curve with a position, width, and temperature dependence that contrast with the data shown here.

function.[10]

Raman spectra of doped semiconductors reveal electronic valley orbit transitions in cases with anisotropic effective masses. Interesting plasmon-phonon line shapes have been observed,[16,17] and a broad continuum occurs in n-type SiC. Broad Raman peaks in doped silicon and germanium reveal line shapes and intensities that change with carrier concentration and applied pressure in a manner that is compatible with light coupling to intervalley density fluctuations.[18] This scattering appears as a Lorentzian-like tail whose width is dominated by impurity scattering.[19] Coupling to an Einstein phonon introduces a predominant peak at the phonon frequency.[20] Interband transitions have been proposed[21] to explain low-frequency Raman structure in the superconducting state of certain copper oxides. However, none of these sources are expected to generate a smooth spectrum extending to 1 eV as seen in the cuprates.

Hence we proceed to calculate the energy fluctuation response using the NFL analysis for electron-electron scattering. The formalism is presented in Sec. II, and a comparison to Raman data on high-temperature superconductors is in Sec. III. Conclusions of our study with suggested prospects for similar nesting phenomena in chromium, transition-metal alloys, and various rare-earth metals are presented in Sec. IV.

II. FORMALISM

Light coupling to electrons via the vector potential $\mathbf{A}$ can be treated in second-order perturbation theory to

derive a cross section:[22]

$$I_R = r_0^2 \frac{\omega_s}{\omega_i} \tilde{S}(\mathbf{q},\omega) , \tag{5}$$

where $r_0 = e^2/mc^2$ is the Thomson radius, and $\omega_i(\omega_s)$ is the incident (scattered) light frequency. The generalized structure factor is defined as

$$\tilde{S}(\mathbf{q},\omega) = (1-e^{-\omega/T})^{-1} \mathrm{Im}\tilde{\chi}(\mathbf{q},\omega) , \tag{6}$$

with

$$\tilde{\chi}(\mathbf{q},\omega) = \langle [\tilde{\rho}(\mathbf{q}),\tilde{\rho}(-\mathbf{q})] \rangle(\omega) , \tag{7}$$

where $\mathbf{q}$ and ω represent the momentum and energy transfer of the scattered photon, respectively. The effective density

$$\tilde{\rho}(\mathbf{q}) = \sum_{\mathbf{k}\sigma} \gamma(\mathbf{k}) c^{\dagger}_{\mathbf{k}+\mathbf{q},\sigma} c_{\mathbf{k},\sigma} \tag{8}$$

involves the energy fluctuations that are vital in the present case of anisotropic Fermi surface scattering and $c^{\dagger}_{\mathbf{k}\sigma}$ ($c_{\mathbf{k}\sigma}$) represent creation (destruction) operators for electrons. The momentum-dependent function $\gamma(\mathbf{k})$ depends on the scattering geometry through the polarization vectors of the incoming (e^i_β) and scattered (e^s_α) light:

$$\gamma(\mathbf{k}) = \sum_{\alpha,\beta} e^s_\alpha \gamma_{\alpha\beta}(\mathbf{k}) e^i_\beta . \tag{9}$$

For nonparabolic energy dispersion $E(\mathbf{k})$ the generalized inverse mass tensor $\gamma_{\alpha\beta}(\mathbf{k})$ reduces to $m_0 \partial^2 E(\mathbf{k}) \partial k_\alpha \partial k_\beta$ if the incoming and scattered light frequencies are neglected in comparison to the optical band gap,[7,8] and m_0 denotes the free-electron mass.

The effective density correlation function with both self-energy and vertex corrections can be expressed as

$$\tilde{\chi}(\mathbf{q},i\nu) = \frac{1}{(2\pi)^3} \int d^3k \, T \sum_{\omega} \gamma(\mathbf{k}) G(\mathbf{k}+\mathbf{q}/2, i\omega) G(\mathbf{k}-\mathbf{q}/2, i(\omega-\nu)) V(\mathbf{k},i\omega;\mathbf{q},i\nu) . \tag{10}$$

Our treatment is based on the NFL approach[11] used previously to calculate the optical conductivity.[12] The key physical input is that the response of a nested Fermi surface is dominated by correlations with a typical nesting wave vector $\mathbf{Q}$. Then the electron-electron scattering yields a quasiparticle self-energy

$$\Sigma(\mathbf{k},i\omega) = \frac{1}{(2\pi)^3} \int d^3p \, T \sum_{\omega'} K[\mathbf{k}-\mathbf{p}, i(\omega-\omega')] G(\mathbf{p},i\omega') , \tag{11}$$

where the corresponding diagrams are shown in Fig. 2. Considering an electron-electron coupling $g \equiv U\Omega$, in terms of the on-site Coulomb repulsion U and unit cell volume Ω, the basic interaction kernel becomes

$$K(\mathbf{p},i\nu) \cong g^2 \chi_{\mathrm{NFL}}(\mathbf{Q},i\nu) , \tag{12}$$

where the susceptibility χ_{NFL} includes self-energy corrections in the electron-hole propagation.

Within these approximations, Eqs. (11) and (12) yield the self-energy and analytic continuation gives a quasiparticle damping[11]

$$\Gamma_{\mathrm{NFL}}(\omega) = -\Sigma''_{\mathrm{NFL}}(\omega) = \alpha \max(\beta T, |\omega|) , \tag{13}$$

where β is of order unity and the coefficient α increases with the dimensionless coupling $\bar{g} = gN(0) \approx U/W$ to values approaching unity when $\bar{g} \sim 1$, i.e., when U is nearly equal to the bandwidth W. This quasiparticle damping rate should not be confused with the transport relaxation rate discussed in the Introduction. We show later that an additional momentum dependence in the kernel K does not spoil the linear frequency and temperature dependence of the self-energy.

The vertex corrections are represented by diagrams in Fig. 3, and they involve the same kernel $K(i\nu)$ defined in Eq. (12). In addition we consider corrections caused by the long-range Coulomb coupling $V_q = 4\pi e^2/q^2$, which yields the total vertex

$$V(\mathbf{k},i\omega;\mathbf{q},i\nu) = \gamma(\mathbf{k}) + V_c(\mathbf{q},i\nu) + \tilde{V}(\mathbf{k},i\omega;\mathbf{q},i\nu) , \tag{14}$$

where

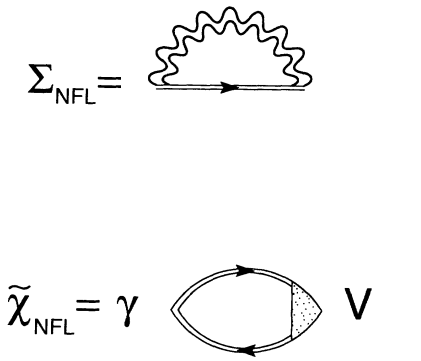

FIG. 2. Quasiparticle self-energy Σ_{NFL} with the double lines representing dressed propagators that include self-energy corrections in a self-consistent way. The double wavy line is the kernel K which originates from electron-electron scattering with momenta near the nesting wave vector $\mathbf{Q}$. The shaded triangle is the vertex V and the effective density response function $\tilde{\chi}_{\mathrm{NFL}}(\mathbf{q} \simeq 0, \omega)$ includes the photon coupling γ to the energy-density fluctuations.

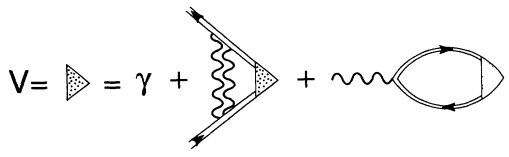

FIG. 3. Diagrammatic representation of the vertex equation that includes the light coupling γ to the energy fluctuations, the electron-electron scattering kernel K (double wavy lines), and the long-range Coulomb interaction shown as a single wavy line.

$$\tilde{V}(k,i\omega;\mathbf{q},i\nu)=[1/(2\pi)^3]\int d^3p\, T\sum_{\omega'} K[\mathbf{k}-\mathbf{p},i(\omega-\omega')]G(\mathbf{p}+\mathbf{q}/2,i\omega')G(\mathbf{p}-\mathbf{q}/2,i(\omega'-\nu))V(\mathbf{p},i\omega';\mathbf{q},i\nu) \quad (15)$$

and

$$V_c(q,i\nu)=[V_q/(2\pi)^3]\int d^3pT\sum_{\omega'} G(\mathbf{p}+\mathbf{q}/2,i\omega')G(\mathbf{p}-\mathbf{q}/2,i(\omega'-\nu))V(\mathbf{p},i\omega';\mathbf{q},i\nu)\ . \quad (16)$$

We note that $K(\mathbf{q}, i\nu\rightarrow\infty)=0$ and therefore $\tilde{V}(k,i\omega\rightarrow\infty;\mathbf{q}i\nu)=0$ as well.

Hence determination of the Raman cross section requires a self-consistent solution of these self-energy and vertex equations. To treat these coupled equations we expand the $\mathbf{k}$-dependent functions in terms of a complete orthonormal set of Fermi surface harmonics $\varphi_L(\mathbf{k})$,[23] with $\varphi_{L=0}(\mathbf{k})=1$ and

$$\gamma(\mathbf{k})=\sum_L \gamma_L\varphi_L(\mathbf{k})\ , \quad (17)$$

$$V(\mathbf{k},i\omega;\mathbf{q},i\nu)=\sum_L V_L(i\omega;\mathbf{q},i\nu)\varphi_L(\mathbf{k})\ , \quad (18)$$

and

$$K[\mathbf{k}-\mathbf{p},i(\omega-\omega')]=\sum_{L,M} K_{L,M}[i(\omega-\omega')]\varphi_L(\mathbf{k})\varphi_M(\mathbf{p})\ . \quad (19)$$

For simplicity we approximate the kernel in a diagonal form

$$K_{L,M}(i\nu)=K_L(i\nu)\delta_{LM}\ , \quad (20)$$

thereby restricting but not eliminating its momentum dependence. The constant component $K_0(i\nu)$ then corresponds to the momentum-independent approximation of Eq. (12) which was used in Ref. 12. By a similar analysis to the conductivity derivation,[12] the decomposition of Eq. (18) and the condition of Eq. (20) yield a momentum-independent self-energy

$$\Sigma(i\omega)=-i\,\mathrm{sgn}(\omega)\Gamma(i\omega)\ , \quad (21)$$

with

$$\Gamma(i\omega)=\pi N(0)T\sum_{|\nu|<|\omega|} K_0(i\nu)\ , \quad (22)$$

providing that the electron density of states $N(E)\cong N(0)$ is slowly varying near the Fermi energy. Using $K_0(i\nu)$ and the nesting approximation for the quasiparticle energy $E(\mathbf{k}+\mathbf{Q})\cong -E(\mathbf{k})$ produces the NFL damping[11] in Eq. (13).

We note that the approximation of a diagonal kernel in Eq. (20) facilitates the analytic approach of calculating correlation functions in this paper. Allowing off-diagonal terms in K leads to a momentum-dependent self-energy via Eq. (11), and then the resulting nonlinear equation requires numerical analysis. Recent computations[24] on a two-dimensional (2D) Hubbard model with the NRL connection machine indeed show momentum variations in the self-energy, which may suggest 25–30 % corrections to the averaged constant term over the whole Brillouin zone. Nevertheless the qualitative strength and, most important, the frequency variation of the NFL self-energy is confirmed by these sophisticated self-consistent numerical results in the case of a nearly half-filled band which exhibits nesting of the Fermi surface. Therefore the present derivation of the long-wavelength response should capture the essence of the line shape by using the leading term in the self-energy.

Turning to the effective density response $\tilde{\chi}$, we realize that the Green's function

$$G^{-1}(\mathbf{k}+\mathbf{q}/2,i\omega)=i\omega-E(\mathbf{k}+\mathbf{q}/2)-\Sigma(i\omega) \quad (23)$$

can be reduced (by noting the smallness of the light momentum $\mathbf{q}$) to

$$G^{-1}(\mathbf{k}+\mathbf{q}/2,i\omega)\cong i\omega-E(\mathbf{k})-\mathbf{q}\cdot\mathbf{v}_F(\mathbf{k})/2+i\,\mathrm{sgn}(\omega)\Gamma(i\omega)\ . \quad (24)$$

Considering the laser frequencies and Fermi velocity $\mathbf{v}_F$ appropriate for cuprate superconductors, $\mathbf{q}\cdot\mathbf{v}_F\simeq 30$ cm^{-1}, while the lowest value of the damping is $\Gamma(\omega=0)\simeq T>T_c\sim 100$ cm^{-1}. Hence it is sensible to take $\mathbf{q}\rightarrow\mathbf{0}$ in the evaluation of $\tilde{\chi}$, and $\tilde{V}$ from Eqs. (10) and (15). At this stage our analysis departs from previous calculations[7] because the predominant influence of the frequency-dependent damping will greatly extend the range of the NFL Raman cross section.

Using the Fermi-surface harmonics we thus obtain

$$\tilde{\chi}(\mathbf{q},i\nu)=N(0)\sum_L\gamma_L\int dE T\sum_\omega \frac{V_L(i\omega;\mathbf{q},i\nu)}{i\,\mathrm{sgn}(\omega)[|\omega|+\Gamma(i\omega)]-E}\,\frac{1}{i\,\mathrm{sgn}(\omega-\nu)\{|\omega-\nu|+\Gamma[i(\omega-\nu)]\}-E}\ . \quad (25)$$

The lack of absolute convergence of Eq. (25) requires care in the interchange of the energy integral and sum.[25] In the process the condition

$$V_L(i\omega\rightarrow\infty;\mathbf{q},i\nu)=\gamma_L+\delta_{L,0}V_c(q,i\nu) \quad (26)$$

enters and reduces Eq. (25) to

$$\tilde{\chi}(\mathbf{q},i\nu)=N(0)\sum_L\gamma_L\left[\gamma_L+\delta_{L,0}V_c(q,i\nu)-2\pi T\sum_{0<\omega<\nu}\frac{V_L(i\omega;\mathbf{q},i\nu)}{\nu+\Gamma(i\omega)+\Gamma[i(\nu-\omega)]}\right]\ . \quad (27)$$

Similar treatment of the vertex equation (14) yields

$$V_L(i\omega;\mathbf{q},i\nu)=\gamma_L+\delta_{L,0}V_c(\mathbf{q},i\nu)+2\pi T\sum_{0<\omega'<\nu}\frac{N(0)K_L[i(\omega-\omega')]}{\nu+\Gamma(i\omega')+\Gamma[i(\nu-\omega')]}V_L(i\omega';\mathbf{q},i\nu)\ . \tag{28}$$

Since the long-range Coulomb interaction couples only to the long-wavelength density fluctuations, it contributes corrections only in the $L=0$ channel in Eqs. (27) and (28). The vertex equation (28) in the $L=0$ channel is solved by summing over the range $0<\omega<\nu$ and using the identity[12]

$$2\pi T\sum_{0<\omega<\nu}N(0)K_0[i(\omega-\omega')]=\Gamma(i\omega')+\Gamma[i(\nu-\omega')]\ , \tag{29}$$

which gives

$$2\pi T\sum_{0<\omega<\nu}\frac{V_0(i\omega;\mathbf{q},i\nu)}{\nu+\Gamma(i\omega)+\Gamma[i(\nu-\omega)]}=\gamma_0+V_c(q,i\nu)\ . \tag{30}$$

Clearly then, the $L=0$ channel including the Coulomb potential cancels completely in Eq. (27) and thus yields zero contribution to the effective density response $\tilde{\chi}$. This is not surprising since the $L=0$ channel corresponds to the ordinary density fluctuations which obey the f-sum-rule requirement $\chi(\mathbf{q}\to\mathbf{0},\omega)\to 0$.[1] This behavior is a consequence of particle conservation, and is satisfied by the actual density response in the nesting approximation as well.[12]

Finally, the main result of these calculations yields a $\mathbf{q}$ independent Raman cross section that arises from the $L\neq 0$ channels which are not constrained by the f-sum rule.[9,26] The resulting effective susceptibility is

$$\tilde{\chi}(i\nu)=N(0)\sum_{L\neq 0}\gamma_L\left[\gamma_L-2\pi T\sum_{0<\omega<\nu}\frac{V_L(i\omega;i\nu)}{\nu+\Gamma(i\omega)+\Gamma[i(\nu-\omega)]}\right]\ , \tag{31}$$

and the vertex function becomes

$$V_L(i\omega;i\nu)=\gamma_L+2\pi T\sum_{0<\omega'<\nu}\frac{N(0)K_L[i(\omega-\omega')]}{\nu+\Gamma(i\omega')+\Gamma[i(\nu-\omega')]}V_L(i\omega';i\nu)\ . \tag{32}$$

III. NFL RAMAN SPECTRUM

A comparison to experimental data on high-temperature superconductors is now feasible with the effective density response from Eqs. (31) and (32) evaluated with the NFL damping of Eq. (13). First we consider the situation where the kernel is presumed to be momentum independent, and then we treat the more general case where the momentum variation may influence the spectral response at different scattering geometries.

A. Momentum independent kernel

Considering electron-electron scattering events characterized by a nesting wave vector $\mathbf{Q}$ to be dominant leads[12] to the simple kernel $K_L(i\nu)=\delta_{L,0}K_0(i\nu)$. Then the vertex of Eq. (32) reduces to $V_L(i\omega;i\nu)=\gamma_L$ for $L\neq 0$, and the correlation function of Eq. (31) becomes

$$\tilde{\chi}(i\nu)=N(0)\sum_{L\neq 0}\gamma_L^2\left[1-2\pi T\sum_{0<\omega<\nu}\frac{1}{\nu+\Gamma(i\omega)+\Gamma[i(\nu-\omega)]}\right]\ . \tag{33}$$

A similar frequency sum was encountered in the treatment[12] of the NFL optical conductivity, where it was shown that $\Gamma(i\omega)+\Gamma[i(\nu-\omega)]$ can be replaced by its average value

$$\bar{\Gamma}(i\nu)=\frac{2\pi T}{\nu}\sum_{0<\omega<\nu}\{\Gamma(i\omega)+\Gamma[i(\nu-\omega)]\}\ , \tag{34}$$

due to the weak frequency dependence in the range $0<\omega<\nu$. Thus we obtain

$$\tilde{\chi}(i\nu)=N(0)\sum_{L\neq 0}\gamma_L^2\frac{\bar{\Gamma}(i\nu)}{\nu+\bar{\Gamma}(i\nu)}\ . \tag{35}$$

By analogy to the conductivity calculation,[12] analytic continuation and the causality requirement for the response yield real and imaginary parts of $\bar{\Gamma}$ that determine the transport lifetime $\tau_{\rm NFL}(\omega,T)$ given in Eq. (4) and the corresponding mass normalization

$$\frac{m^*_{\rm NFL}}{m_0}(\omega,T)=1+\frac{2\alpha}{\pi}\ln\left[\frac{\omega_c}{\max(\beta' T,|\omega|)}\right]\ . \tag{36}$$

Finally the Raman cross section follows from Eqs. (5), (6), (35), and (36), and is

$$I_{\rm NFL}=r_0^2\frac{\omega_s}{\omega_i}N(0)[1-e^{-\omega/T}]^{-1}\times\sum_{L\neq 0}\gamma_L^2\frac{\omega\tau_{\rm NFL}(\omega)}{[m^*_{\rm NFL}(\omega)/m_0]^2\omega^2\tau^2_{\rm NFL}(\omega)+1}\ . \tag{37}$$

Some qualitative features of this spectrum are apparent from Eq. (37). At low temperatures the relaxation time is roughly $\tau_{\rm NFL} \cong (\alpha\beta'\omega)^{-1}$ over the frequency range $\omega > \beta' T$ and $\omega > \omega^*$ so that the only frequency variation of the NFL Raman spectrum is caused by the weak frequency variation of the effective mass $m^*_{\rm NFL}(\omega, T)$: A crossover to conventional Fermi liquid behavior should occur below $\omega^* \cong \beta' T^*$, where $\beta' \simeq 3.3$ and T^* is estimated near 100 K from numerical calculations with realistic tight-binding bands.[27,28] Thus variations in the electron-electron coupling which are proportional to α tend to change the overall intensity of the spectrum but will have relatively small influence on $m^*(\omega)$ and thus will not change the overall shape of the Raman spectrum, which is rather smooth in any event. Hence changes in the Fermi surface nesting induced by oxygen doping, for example, are not expected to give dramatic line-shape changes unless of course the nesting is substantially destroyed.

A remarkable correlation appears between the Raman line shape $I_{\rm NFL}$ and the optical conductivity[12]

$$\sigma_{\rm NFL}(\omega) = \frac{1}{4\pi} \frac{\omega_{\rm pl}^2 \tau_{\rm NFL}(\omega)}{[m^*_{\rm NFL}(\omega)/m_0]^2 \omega^2 \tau^2_{\rm NFL} |\omega| + 1} , \tag{38}$$

which allows Eq. (37) to be rewritten as

$$I_{\rm NFL} = r_0^2 (\omega_s/\omega_i)(1 - e^{-\omega/T})^{-1} N(0) \times \sum_{L \neq 0} \gamma_L^2 (4\pi/\omega_{\rm pl}^2) \omega \sigma_{\rm NFL}(\omega) . \tag{39}$$

This surprising proportionality between the Raman line shape and the conductivity is very much different from the traditional isotropic Raman cross-section result[1] of Eq. (1) and is generally not valid for a nonparabolic band with weak damping.[7]

The proportionality of the Raman spectrum and the conductivity was anticipated previously[9] in the theory of Mott-Hubbard systems with a similar "stress tensor" analysis for the light coupling to energy fluctuations. However, the origin of the anomalous Raman scattering was attributed to "incoherent" parts of the spectral representation without specifying its frequency distribution. Physically a rough proportionality is expected when the nonparabolicity of the band induces light coupling to nonconserved density fluctuations providing that the matrix elements[8] of this process are comparable to the true current operator which determines the conductivity.

A comparison of the NFL Raman line shape to data[6] on $YBa_2Cu_3O_7$ is shown in Fig. 4, using the interpolation formulas

$$1/\tau_{\rm NFL} = \alpha[(\beta' T)^2 + \omega^2]^{1/2} \tag{40a}$$

and

$$\frac{m^*_{\rm NFL}}{m_0} = 1 + \frac{2\alpha}{\pi} \ln \left[\frac{\omega_c}{[(\beta' T)^2 + \omega^2]^{1/2}} \right] , \tag{40b}$$

with $\beta' = 3.3$. These expressions have the appropriate NFL asymptotic limits of Eq. (4) at $T \ll \omega$ and also $T \gg \omega$. However, the validity of these expressions is also subject to the constraint $\omega > \omega^* > 3T^*$ which marks the crossover to conventional Fermi-liquid behavior that is expected for a realistic band structure such as in Ref. 28. The predicted sharp upturn at very low frequencies in the NFL spectrum using Eq. (40) may provide clues to the crossover value ω^*, since the logarithmic divergence of the effective mass in the NFL approximation is removed below ω^*. A rather good description is achieved witih a coupling $\alpha = 0.55$ and a cutoff frequency $\omega_c \cong 17\,000$ $\rm cm^{-1}$ (~ 2 eV) which were obtained from our earlier analysis[14] of the reflectivity of untwinned single crystals. The variation of the NFL spectrum is also shown for another value of the coupling α to illustrate the weak sensitivity of the line shape.

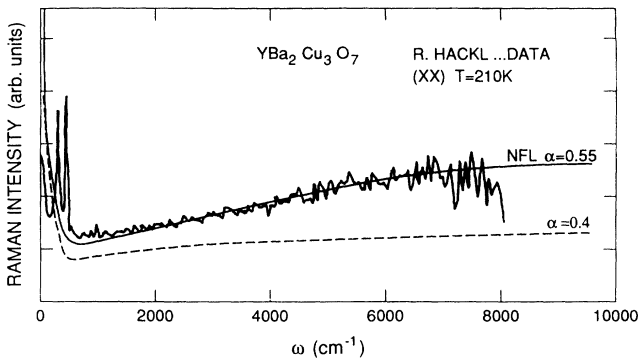

FIG. 4. The calculated NFL Raman line shape yields the solid curve for $\alpha = 0.55$ and $\omega_c = 17\,000$ $\rm cm^{-1}$ (≈ 2 eV), which were obtained from our previous analysis of optical conductivity and reflectance of $YBa_2Cu_3O_7$ in Ref. 14. The Raman data of Staufer, Hackl, and Müller of Ref. 6 for the (XX) polarization shows the slight frequency upturn in accord with the theory for a single scattering channel.

The Raman data[6] for $Bi_2Sr_2CaCu_2O_8$ also agrees with the NFL spectrum in Fig. 5 using the parameters $\alpha = 0.4$ and $\omega_c = 10\,000$ $\rm cm^{-1}$ from our previous fits[14] to the

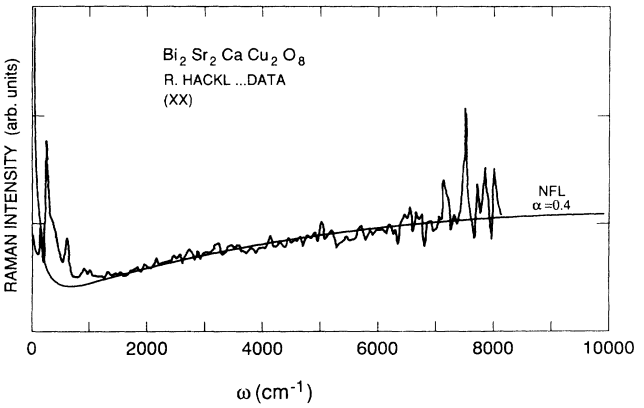

FIG. 5. Raman spectrum of $Bi_2Sr_2CaCu_2O_8$ from Staufer, Hackl, and Müller in Ref. 6 is compared to the NFL line shape calculated using $\alpha = 0.4$ and $\omega_c = 1.2$ eV. These parameters are identical to the values which were found earlier in the NFL analysis of optical conductivity (Ref. 14) and also are compatible with the structure factor shown in Fig. 1 along with the f-sum rules. The data and analysis are done at $T = 120$ K.

reflectivity, conductivity, and structure factor of this high-temperature superconductor.

There remains the problem of spectral changes observed in the cuprates at different polarizations. To examine these features, we consider next an appropriate solution of the vertex equation (32) when the momentum dependence of the kernel gives $K_L \neq 0$ for $L=0$.

B. Momentum dependence and scattering geometry

To achieve a tractable analytic solution for the vertex in Eq. (32) we assume that the frequency dependence of the kernel is the same for all channels with a magnitude λ_L; i.e., $K_L(i\nu) \cong \lambda_L K_0(i\nu)$, where $\lambda_0=1$. It seems reasonable to take $|\lambda_{L\neq 0}|<1$ because $K(\mathbf{q},i\nu)>0$. In fact λ_L may be much less than 1 in most channels because the kernel K_0 of Eq. (12) is found to be an order of magnitude larger than a conventional Fermi-liquid average that should represent non-nested regions of the Fermi surface. The generalized susceptibility becomes

$$\tilde{\chi}(i\nu)=N(0)\sum_{L\neq 0}\gamma_L^2\frac{(1-\lambda_L)\bar{\Gamma}(i\nu)}{\nu+1(1-\lambda_L)\bar{\Gamma}(i\nu)} . \tag{41}$$

Evidently the functional form is modified slightly by contributions from different channels. For $\lambda_L>0$ the effective slope of the Raman spectrum decreases, while for $\lambda_L<0$ the slope increases. However, multichannel scattering contributions to the Raman cross section I_{NFL} are not simply related to the optical conductivity $\sigma(\omega)$. Hence the approximate proportionality $I_{\mathrm{NFL}} \propto (1-e^{-\omega/T})^{-1}\omega\sigma_{\mathrm{NFL}}(\omega)$ that appears to be compatible with the data for the cuprates in Figs. 4 and 5 may indicate that the momentum-independent $L=0$ channel dominates the scattering in $Bi_2Sr_2CaCu_2O_8$ and in $YBa_2Cu_3O_7$.

Since different scattering geometries sample different sets of γ_L, the frequency dependence of Eq. (41) will depend slightly on the polarization of the light, because the functions containing λ_L will enter with different weights.

C. Low-temperature limit

At frequencies above the phonon range, i.e., $\omega>1000$ cm^{-1}, the NFL spectrum exhibits negligible temperature variation as seen in Fig. 6.

In the phonon range strong antiresonance line shapes near the phonon peaks are observed,[2-6] and these suggest an interference between the ion response and the electronic continuum. In addition there is inevitably strong Rayleigh scattering at the lowest frequencies which masks the temperature dependence as well. Nevertheless it may be worthwhile to search more closely the low-frequency region for indications and limits of the low-frequency upturn predicted by Eqs. (38) and (39), and shown in Fig. 6.

The high transition temperatures of the cuprates impose another lower limit on our frequency analysis which is valid for the normal state. The creation of a superconducting energy gap may also modify the nesting features of the Fermi surface. Attempts to deduce a gap from an examination of the temperature variation of the spectrum

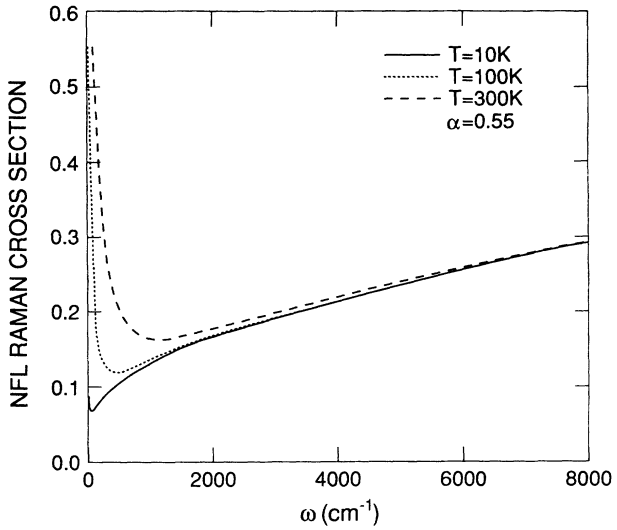

FIG. 6. The calculated Raman line shape $\tilde{S}_{\mathrm{NFL}}$ in the single-channel NFL analysis is shown for three different temperatures to illustrate the uptrend at low frequencies caused by the temperature and frequency variation of the effective mass $m^*_{\mathrm{NFL}}(\omega,T)$. Experimental data in the low-frequency region show phonon peaks and pronounced interference line shapes as in Figs. 4 and 5. Also Rayleigh scattering at very low frequencies may mask the unusual temperature-dependent structure predicted by the NFL theory.

at low frequencies may well be complicated by the additional variation of the NFL electronic scattering shown in Fig. 6.

A fundamental theoretical issue is the validity of a Fermi-liquid description for the copper oxide superconductors. The "marginal" FL hypothesis asserts that the effective mass $m^*(T,\omega)$ that is deduced from a phenomenological form[10] of the susceptibility and damping rate exhibits a logarithmic singularity in temperature which leads to a breakdown of the concept of well-defined quasiparticles. This type of situation occurs for an electron gas in one dimension, and also has been proposed in the original formulation of the spinon-holon excitation spectrum[29] for a doped highly correlated Mott-Hubbard insulator.

Our nested formulation avoids these difficulties at the lowest temperatures even though the functional dependence of $m^*_{\mathrm{NFL}}(\omega,T)$ in Eq. (36) is similar to the results of the "marginal" FL approach.[10] Since the nesting is not perfect, there will be a crossover temperature T^* and frequency ω^* below which the quasiparticle is so narrowly confined to the orbit that the trajectory curvature fails to satisfy the nesting condition and the response reverts to a conventional Fermi liquid.

Numerical computations[27] of the susceptibility and quasiparticle self-energy verify the crossover from NFL response at reasonable values of T^* and ω^*, provided that the input of two-dimensional tight-binding bands is tailored to fit the Fermi surfaces predicted by band-structure calculations.[28] It is noteworthy that the band calculations show substantial Fermi-surface nesting for

essentially all of the high-temperature superconductors examined so far.

IV. CONCLUSIONS

Light scattering by energy fluctuations in a nonparabolic conduction band is shown to yield a broad continuum which may extend to 8000 cm^{-1} or roughly 1 eV in the case of substantial nesting of the Fermi surface. A remarkable proportionality of the Raman cross section to the optical conductivity in our NFL analysis is found for the simplest approximation of the electron-electron scattering kernel. Quantitative evidence for such unusual behavior is provided by the good fits achieved for the Raman spectra of $YBa_2Cu_3O_7$ and $Bi_2Sr_2CaCu_2O_8$ using parameters determined previously from our NFL analysis of optical conductivity and reflectivity data for these superconductors.

Nested Fermi surfaces are expected to occur in various rare-earth metals and in transition metals such as chromium. Thus it is encouraging that a broad Raman continuum has been observed in Dy, Er, and Y films,[30] and independent evidence for a linear frequency variation of the quasiparticle damping is apparent in the infrared reflectivity measurements[31] on Ba, Sr, Eu, and Yb, and also in chromium.[32]

Since nesting is known to influence the range, sign, and periodicity of the indirect exchange coupling between localized spins that is mediated by conduction electrons, optical investigations may reveal clues to the origin of magnetic ordering phenomena in transition-metal alloys and in multilayer films.

Our theoretical formulation for the NFL self-energy and vertex corrections satisfies the Ward identity required for charge conservation and gauge invariance.[33] However, the treatment of the light coupling vertex to the anisotropic energy fluctuations yields a Raman cross section that is much larger than the conventional particle-hole process. The latter scattering vanishes as the square of the light momentum transfer as required by particle conservation and the Pauli exclusion principle, and hence is extremely small for the applicable laser frequencies. By contrast, the anomalous Raman spectrum derived for a nested Fermi surface yields strong intensity and polarization properties that are sensitive to details of the energy-momentum dispersion, while the actual density response is nevertheless compliant with charge conservation.

ACKNOWLEDGMENTS

One of the authors (A.V.) wishes to thank R. Hackl and his colleagues at the Walther-Meissner-Institute für Tieftemperaturforschung for their hospitality. We appreciate the advice and encouragement from A. Zawadowski, and valuable discussions with R. Hackl, M. V. Klein, B. S. Shastry, K. Itai, and R. F. Wallis. We thank J. Zhang for technical assistance. This research is supported by DOE Grant No. DE-FG05-91ER45113, and by the Hungarian National Research Fund No. OTKA 1787.

[1]D. Pines and P. Nozières, *Theory of Quantum Liquids* (Benjamin, Reading, MA, 1966).

[2]S. L. Cooper, F. Slakey, M. V. Klein, J. P. Rice, E. D. Bukowski, and D. M. Ginsberg, Phys. Rev. B **38**, 11 934 (1988).

[3]F. Slakey, S. L. Cooper, M. V. Klein, J. P. Rice, and D. M. Ginsberg, Phys. Rev. B **39**, 2781 (1989).

[4]K. B. Lyons and P. A. Fleury, J. Appl. Phys. **64**, 6075 (1988).

[5]S. Sugai, Y. Enomoto, and T. Murakami, Solid State Commun. **72**, 1193 (1989).

[6]T. Staufer, R. Hackl, and P. Müller, Solid State Commun. **75**, 975 (1990); Solid State Commun. **79**, 409 (1991).

[7]P. A. Wolff, Phys. Rev. **171**, 436 (1968), and cited references therein to data on doped semiconductors.

[8]A. A. Abrikosov and V. M. Genkin, Zh. Eksp. Teor. Fiz **65**, 842 (1973) [Sov. Phys. JETP **38**, 417 (1974)].

[9]B. S. Shastry and B.I. Shraiman, Phys. Rev. Lett. **65**, 1068 (1990).

[10]C. M. Varma, P. B. Littlewood, S. Schmitt-Rink, E. Abrahams, and A. E. Ruckenstein, Phys. Rev. Lett. **63**, 1996 (1989).

[11]A. Virosztek and J. Ruvalds, Phys. Rev. B **42**, 4064 (1990).

[12]J. Ruvalds and A. Virosztek, Phys. Rev. B **43**, 5498 (1991).

[13]K. Kamarás *et al.*, in *Electronic Properties of High Temperature Superconductors*, edited by H. Kuzmany *et al.*, Solid State Sciences Vol. 99 (Springer, Berlin, 1990), p. 260.

[14]J. Ruvalds, J. Zhang, and A. Virosztek (unpublished).

[15]N. Nücker, H. Romberg, S. Nakai, B. Scheerer, J. Fink, Y. F. Yan, and Z. X. Zhao, Phys. Rev. B **39**, 12 379 (1989).

[16]G. B. Wright and A. Mooradian, Phys. Rev. Lett. **18**, 608 (1967).

[17]Priscilla J. Colwell and Miles V. Klein, Phys. Rev. B **6**, 498 (1972).

[18]G. Contreras, A. K. Sood, and M. Cardona, Phys. Rev. B **32**, 924 (1985); **32**, 930 (1985).

[19]A. Zawadowski and M. Cardona, Phys. Rev. B **42**, 10 732 (1990).

[20]K. Itai (unpublished).

[21]H. Monien and A. Zawadowski, Phys. Rev. Lett. **63**, 911 (1989).

[22]M. V. Klein and S. B. Dierker, Phys. Rev. B **29**, 4976 (1984).

[23]P. B. Allen, Phys. Rev. B **13**, 1416 (1976).

[24]D. W. Hess, and J. W. Serene (unpublished); J. W. Serene and D. W. Hess, Phys. Rev. B **44**, 3391 (1991).

[25]See, for example, A. A. Abrikosov, L. P. Gorkov, and I. E. Dyzaloshinski, *Methods of Quantum Field Theory in Statistical Physcis* (Dover, New York, 1975), p. 312.

[26]J. Kosztin and A. Zawadowski (unpublished).

[27]S. Wermbter and L. Tewordt, Phys. Rev. B **43**, 10 530 (1991).

[28]J. Yu, A. F. Freeman, and J. H. Xu, Phys. Rev. Lett. **58**, 1035 (1987); J. Yu *et al.*, Phys. Lett. A **122**, 203 (1987).

[29]P. W. Anderson, Science **235**, 1196 (1987); Phys. Rev. Lett. **64**, 1839 (1990); **65**, 2306 (1990).

[30]R. T. Demers, S. Kong, M. V. Klein, R. Du, and C. P. Flynn, Phys. Rev. B **38**, 11 523 (1988).

[31]J. G. Endriz and W. E. Spicer, Phys. Rev. B **2**, 1466 (1970).

[32]A. S. Barker, Jr. and J. A. Ditzenberger, Phys. Rev. B **1**, 4378 (1970).

[33]See, for example, J. R. Schrieffer, *Superconductivity* (Benjamin, New York, 1964), Chap. 8.